Elsevier Editorial System(tm) for Journal of Non-Crystalline Solids + OA Mirror
Manuscript Draft

Manuscript Number: NOC-D-19-00579R1

Title: Eu3+ ion distribution in oxyfluoride glass nanocomposites

Article Type: Full Length Article

Keywords: transparent oxyfluoride glass ceramics; activator distribution; optical spectroscopy; X-ray diffraction; electron paramagnetic resonance

Corresponding Author: Dr. Andris Antuzevics,

Corresponding Author's Institution: Institute of Solid State Physics, University of Latvia

First Author: Andris Antuzevics

Order of Authors: Andris Antuzevics; Guna Krieke; Elina Pavlovska; Uldis Rogulis

Abstract: Assessment of activator distribution in lanthanide doped nanocomposites is an important and challenging task. Oxyfluoride glass ceramics have been chosen as a model system to characterize incorporation efficiency of Eu3+ ions in CaF2 nanocrystals using a combination of X-ray diffraction (XRD) and electron paramagnetic resonance (EPR) techniques. Lattice constant changes induced by size mismatch of Eu3+ and Ca2+ ions have been used to evaluate Eu3+ content in CaF2. The distortion of CaF2 lattice due to incorporation of europium ions can be detected from EPR investigations via Gd3+ paramagnetic probe spectra. It is shown that ratio of different symmetry CaF2:Gd3+ centres and linewidth of EPR transitions can be used to monitor europium content in the crystalline phase of glass ceramics.

Cover letter

Dear Editor Prof. Josef W. Zwanziger,

Please consider our revised manuscript "Eu^{3+} ion distribution in oxyfluoride glass nanocomposites" for publication in Journal of Non-Crystalline Solids.

We highly appreciate the constructive and helpful comments of the reviewers and have modified the article accordingly. More specifically – we have performed additional electron paramagnetic resonance experiments to evaluate the effect of Eu^{2+} ions in the glass ceramics and investigate the formation of cubic and tetragonal CaF_2:Gd^{3+} centres in more detail. Additionally, we have improved data uncertainty estimates and their descriptions as well as made corrections to the usage of the English language. The changes in the manuscript are highlighted in red font. We believe that the changes have substantially improved the quality of the manuscript.

Thank You for the consideration of our revised manuscript!

Sincerely Yours,

On behalf of all the authors

Dr. Andris Antuzevics

Journal of
Non-Crystalline Solids

Confirmation of Authorship

Please save a copy of this file, complete and upload as the "Confirmation of Authorship" file.

As corresponding author, I Andris Antuzevics, hereby confirm on behalf of all authors that:

1. This manuscript has not been published, was not, and is not being submitted to any other journal. If presented at a conference, the conference is identified. If published in conference proceedings, substantial justification for re-publication must be presented.

2. All necessary permissions for publication were secured prior to submission of the manuscript.

3. All authors listed have made a significant contribution to the research reported and have read and approved the submitted manuscript, and furthermore, all those who made substantive contributions to this work have been included in the author list.

Revision notes

List of changes made to the manuscript (highlighted in red font):

- numerous improvements on the usage of the English language throughout the manuscript;
- updated uncertainty estimates for:
  - Table 2
  - Figure 9
- updated descriptions for uncertainty estimates:
  - for sample weighing precision in “Experimental details”, page 3, paragraph 1;
  - for annealing temperature control precision in “Experimental details”, page 3, paragraph 1;
  - for crystallite size calculation in “Experimental details”, page 3, paragraph 2;
  - for lattice constant calculation in “Experimental details”, page 3, paragraph 2;
  - for luminescence intensity measurements in “Experimental details”, pages 3-4
  - for Eu^{2+} concentration upper limit in “EPR”, page 10, paragraph 2;
  - for Figure 9 in “EPR”, page 12, paragraph 2;
  - for Figure 10 in “EPR”, page 13, paragraph 2;
  - for Table 3 in “EPR”, page 14, paragraph 1;
- added Figure 5, which shows the full XRD patterns of samples annealed at 750 °C;
- added Figure 7, which shows EPR spectra of the S_0 sample annealed at different temperatures;
- changed numeration of the old figures;
- provided additional description about the “U-type” spectrum and references for it in “EPR”, page 10, paragraph 2;
- discussed the formation of cubic and tetragonal CaF_2:Gd^{3+} centres in “EPR”, page 11, paragraph 1.

***Abstract**

Assessment of activator distribution in lanthanide doped nanocomposites is an important and challenging task. Oxyfluoride glass ceramics have been chosen as a model system to characterize incorporation efficiency of Eu^{3+} ions in CaF_2 nanocrystals using a combination of X-ray diffraction (XRD) and electron paramagnetic resonance (EPR) techniques. Lattice constant changes induced by size mismatch of Eu^{3+} and Ca^{2+} ions have been used to evaluate Eu^{3+} content in CaF_2. The distortion of CaF_2 lattice due to incorporation of europium ions can be detected from EPR investigations via Gd^{3+} paramagnetic probe spectra. It is shown that ratio of different symmetry CaF_2:Gd^{3+} centres and linewidth of EPR transitions can be used to monitor europium content in the crystalline phase of glass ceramics.

Highlights

- Eu^{3+} and Gd^{3+} co-doped glass ceramics with CaF_2 nanocrystals have been synthesized.
- Variations in CaF_2 lattice constant are observed if Eu^{3+} incoporate in nanocrytals.
- Gd^{3+} probes are suitable for EPR detection of Eu^{3+} distribution in glass ceramics.
- Tetragonal and cubic CaF_2:Gd^{3+} centre ratio is modified by the presence of Eu^{3+}.
- Gd^{3+} EPR spectra in glass ceramics are broadened by nearby Eu^{3+} ions.

Eu^{3+} ion distribution in oxyfluoride glass nanocomposites

Andris Antuzevics*, Guna Krieke, Elina Pavlovska, Uldis Rogulis
Institute of Solid State Physics, University of Latvia

* Corresponding author
E-mail: andris.antuzevics@cfi.lu.lv

Abstract. Assessment of activator distribution in lanthanide doped nanocomposites is an important and challenging task. Oxyfluoride glass ceramics have been chosen as a model system to characterize incorporation efficiency of Eu^{3+} ions in CaF_2 nanocrystals using a combination of X-ray diffraction (XRD) and electron paramagnetic resonance (EPR) techniques. Lattice constant changes induced by size mismatch of Eu^{3+} and Ca^{2+} ions have been used to evaluate Eu^{3+} content in CaF_2. The distortion of CaF_2 lattice due to incorporation of europium ions can be detected from EPR investigations via Gd^{3+} paramagnetic probe spectra. It is shown that ratio of different symmetry CaF_2:Gd^{3+} centres and linewidth of EPR transitions can be used to monitor europium content in the crystalline phase of glass ceramics.

Keywords: transparent oxyfluoride glass ceramics; activator distribution; optical spectroscopy; X-ray diffraction, electron paramagnetic resonance

1. Introduction

Alkaline earth crystals with fluorite structure are extensively studied as the hosts for doping with rare earth (RE) ions. Among these, calcium fluoride (CaF_2) is an excellent optical material possessing high transparency from infrared to ultraviolet regions of electromagnetic spectrum, low phonon energy and high chemical stability. The interest in CaF_2 containing systems has been stimulated by recent advances in synthesis of nanostructured materials. Nanosized particles have potential to be used as luminescent probes in biomedical imaging [1]; whereas prospective applications of CaF_2 containing nanocomposites range from thin film electrolytes [2] to various types of multifunctional polymer additives [3] and optical devices [4]. CaF_2 nanocomposites doped with RE ions have been widely investigated for optical applications [5–7]. A challenging task arising in the investigation of such multi-phase materials is the quantitative characterization of RE ion distribution.

Considerable attention has been devoted to the investigation of oxyfluoride glass ceramics – nanocomposite systems, in which the selected crystalline phase is surrounded by a chemically stable and thermally durable glass matrix. Moreover, it is possible to retain the transparency of glass by controlling the size of nanocrystals and refractive index of amorphous and crystalline phases. Oxyfluoride glass ceramics can be tailored to comprise fluoride nanocrystals and exhibit efficient luminescence processes [8,9].

Europium doped glass ceramics containing CaF_2 nanocrystals have been investigated recently. Both Eu^{3+} and Eu^{2+} ions are sensitive to crystallization induced local structure changes, which modify luminescence properties – integral intensity, spectral composition and decay time – of the material [10–21]. It has also been observed that crystallization of CaF_2 during the melt cooling process promotes reduction of Eu^{3+} to Eu^{2+} [22]. The magnitude of these effects is expected to be dependent on europium incorporation efficiency in the crystalline phase. Unfortunately, in the above mentioned works the issue of activator distribution between amorphous and crystalline phases has not been addressed.

For a quantitative assessment of activator distribution in glass ceramics several approaches have been used. One of the common techniques is X-ray diffraction (XRD) analysis of lattice constant changes induced by size mismatch between the impurity and host ions [23,24]. More direct visualisations using combined electron microscopy and energy dispersive X-ray spectroscopy techniques can be used to map the elements of interest [25]. If the dependence of a particular luminescence characteristic on the dopant concentration is established, activator distribution can also be assessed from optical spectroscopy measurements [26]. In order to obtain reliable information about activator distribution, a combination of several independent approaches is desirable.

In this work oxyfluoride glass ceramics containing CaF_2 has been selected as a model system to characterize Eu^{3+} ion distribution using XRD and electron paramagnetic resonance (EPR) methods. Gd^{3+} is introduced as a paramagnetic probe to investigate Eu^{3+} ion induced structural changes in the nanocrystals. To the best of our knowledge, activator incorporation efficiency in the crystalline phase of glass ceramics from paramagnetic probe EPR spectra has been evaluated for the first time.

2. Experimental details

Oxyfluoride glasses with nominal compositions shown in Table 1 were synthesized using the melt quenching technique. The chemicals were weighed within a 1 mg precision of the calculated values. Batches of 9 g were melted in covered alumina crucibles at 1400 °C for 1 h. The melts were rapidly cooled by pouring them in stainless steel moulds. The glass ceramics were obtained after 1 h isothermal treatment at selected temperatures. The uncertainty in the annealing temperature due to uneven sample positioning within the furnace was estimated to be approximately ± 10 °C. Additionally, Eu^{3+} and Gd^{3+} doped polycrystalline CaF_2 samples were synthesized following the guidelines described elsewhere [23].

Table 1

Sample	Composition, mol%					
	CaO	CaF_2	Al_2O_3	SiO_2	GdF_3	EuF_3
S_0	8.0	25.9	20.0	46.0	0.1	0.0
S_1	8.0	25.4	20.0	46.0	0.1	0.5
S_2	8.0	24.9	20.0	46.0	0.1	1.0
S_3	8.0	24.4	20.0	46.0	0.1	1.5
S_4	8.0	23.9	20.0	46.0	0.1	2.0
S_5	8.0	20.9	20.0	46.0	0.1	5.0
S_6	8.0	15.9	20.0	46.0	0.1	10.0

XRD data were obtained with Rigaku MiniFlex using Cu K_α tube operated at 40 kV and 15 mA. The mean crystallite size was calculated using the Scherrer equation [27], the uncertainty was estimated to be ± 10 %. The unit cell parameters were calculated using DICVOL06 [28] using Fullprof software [29]. The standard deviation of calculations was less than 0.0005 Å.

The morphology of the samples was examined by scanning electron microscope (SEM) Tescan Lyra operated at 15 kV. Prior to examination, fractured samples were coated with a thin layer of gold.

Luminescence was excited by Xe lamp Hamamatsu C2577 and tunable (210-2300 nm) pulsed EKSPLA NT342/3UV laser (pulse duration ~ 5 ns, repetition frequency 10 Hz). Laser wavelength could be varied by 0.1 nm. Luminescence signal was detected using DU-401 BV CCD camera from Andor and iCCD camera iSTAR DH734_18mm from Andor coupled to Andor SR-303i-B spectrometer. For low temperature measurements samples were placed in a closed cycle He cryostat (Sumitomo DE-204SLFF). For luminescence intensity measurements glass ceramics with different

concentrations of Eu^{3+} were grinded, transferred to transparent glass vials and placed in a stand ensuring an equal positioning of the samples. All samples were measured repeatedly and the confidence interval was estimated using standard deviation and Student's two-sided t-distribution with a significance level of α=0.05.

Room temperature X-band EPR measurements were made on powdered samples using a modified RE 13-06 spectrometer. DPPH reference sample was used for magnetic field calibration. Spectral simulations were performed in EasySpin simulation toolbox [30]. The details of simulations are given in the EPR section of the article.

3. Results and discussion

3.1. General characterization

The glass ceramics were prepared by heat treatment of the precursor glasses. XRD patterns of S_3 samples annealed at different temperatures are shown in Figure 1.

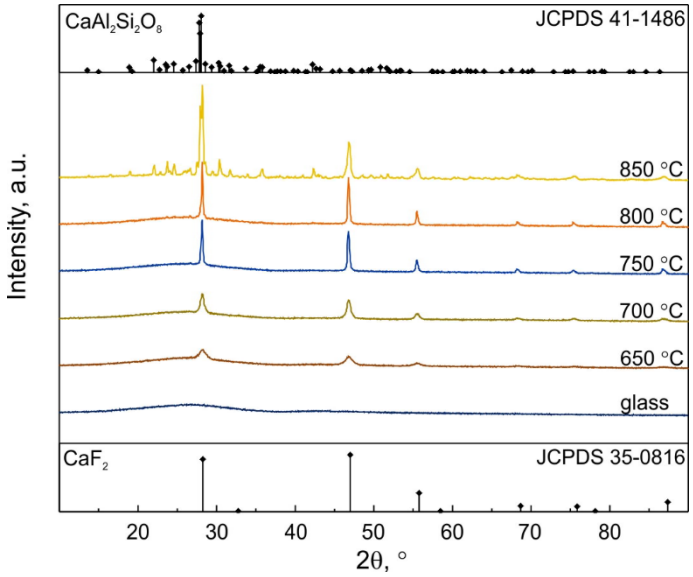

Fig. 1. XRD patterns of S_3 composition samples annealed at different temperatures.

The absence of intense sharp peaks indicates the amorphous nature of the glass sample. The annealed samples exhibit characteristic diffraction patterns of the CaF_2 fluorite structure (JCPDS 35-0816). The intensity of the diffraction peaks is increased after heat treatment at higher temperature indicating the growth of nanocrystals. The average crystallite size has been estimated using the Scherrer equation. The results are given in Table 2. Heat treatment up to 700 °C results in the formation of small

nanocrystals with the average size ranging from 10 to 18 nm; however, heat treatment at higher temperature promotes a rapid increase of crystallite size up to 59 nm.

Table 2

Annealing temperature, °C	Average CaF_2 crystal size, nm
650 ± 10	10 ± 1
700 ± 10	18 ± 2
750 ± 10	46 ± 5
800 ± 10	59 ± 6

In addition, secondary crystalline phases with the most intense peaks matching to anortite $CaAl_2Si_2O_8$ (JCPDS 41-1486) can be detected after heat treatment at temperatures exceeding 800 °C indicating crystallization of the glass matrix. For credible optical spectroscopy and EPR studies glass ceramics with sufficiently large CaF_2 nanocrystals and no additional crystalline phases are required. Therefore, quantitative analysis in this research has been performed on the samples heated at 750 °C for 1 h.

A photograph and SEM micrographs of the S_3 composition samples are shown in Figure 2.

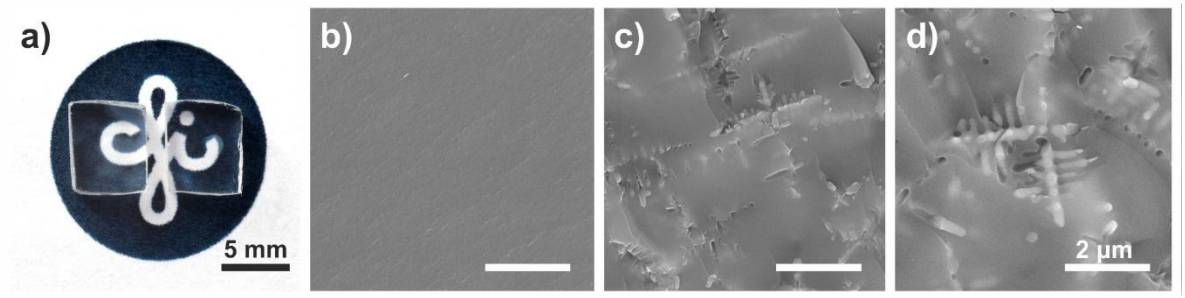

Fig. 2. a) Photograph of S_3 glass and glass ceramics heat treated at 700 °C for 1 h and SEM micrographs of S_3 glass ceramics heat treated at b) 700 °C, c) 750 °C and d) 800 °C for 1h.

Due to the small size of the nanocrystals, the glass and glass ceramics annealed at 700 °C are visually indistinguishable to the naked eye. Annealing at higher temperatures promotes the growth of nanocrystals leading to a more significant scattering of the visible light and overall opaque appearance of the sample. Small, barely detectable nanocrystals are formed in glass ceramics heat treated at 700 °C for 1 h. According to the XRD data, heat treatment at higher temperature promotes a rapid growth of the nanocrystals. Indeed, after heat treatment at 750-800 °C for 1 h large dendritic cubic crystals are formed in the glass matrix. The growth of dendritic crystals suggests relatively low viscosity of the glass matrix, which enables efficient ionic diffusion and rapid crystal growth.

3.2. Optical spectroscopy

Europium ions can exist in two stable valence states – 3+ and 2+ – each having its distinct luminescence properties. Preliminary room temperature optical spectroscopy measurements of our samples revealed Eu^{3+} luminescence in the red spectral region (see inset of Figure 3), while the broad blue emission characteristic to Eu^{2+} in oxyfluoride glasses [11,14,31,32] as well as in CaF_2 crystals [33,34] was not observed in the investigated glass ceramics. Literature is already abundant with room temperature Eu^{3+} luminescence spectra in CaF_2 containing glass ceramics [12,13,17–22], therefore only the novel aspects are emphasized here. Eu^{3+} luminescence intensity in the glass ceramics depending on EuF_3 content in the initial composition is shown in Figure 3. Luminescence is more intense at higher doping levels; however, spectral composition dependence on activator content was determined to be minimal.

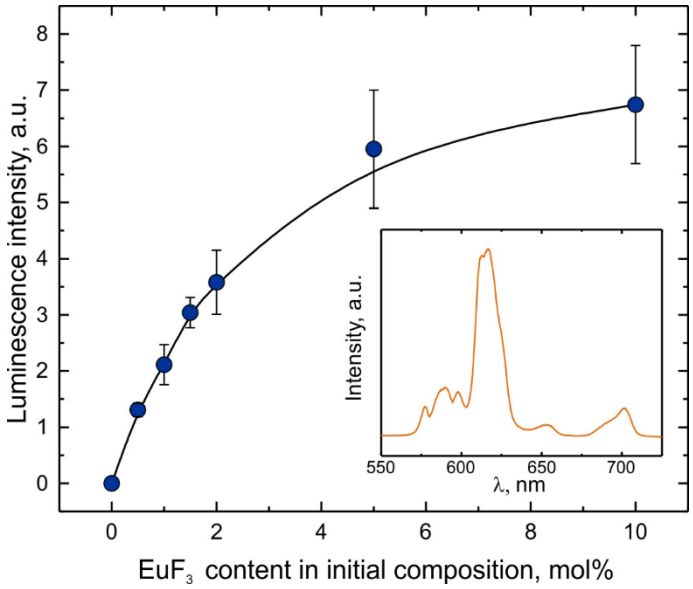

Fig. 3. Intensity of room temperature Eu^{3+} photoluminescence at 612 nm for glass ceramics annealed at 750 °C. Inset shows the photoluminescence spectrum of the S_3 composition sample.

The number of allowed f-f transitions in Eu^{3+} spectrum depends on the symmetry of the surrounding crystal field [35], thus it can be used to probe the structure of solids. Considering this fact, site-selective spectroscopy analysis of glass ceramics was performed at 10 K. The spectra are shown in Figure 4. Two distinct signals, which were absent in the glass samples, could be selectively excited in glass ceramics with low Eu^{3+} content.

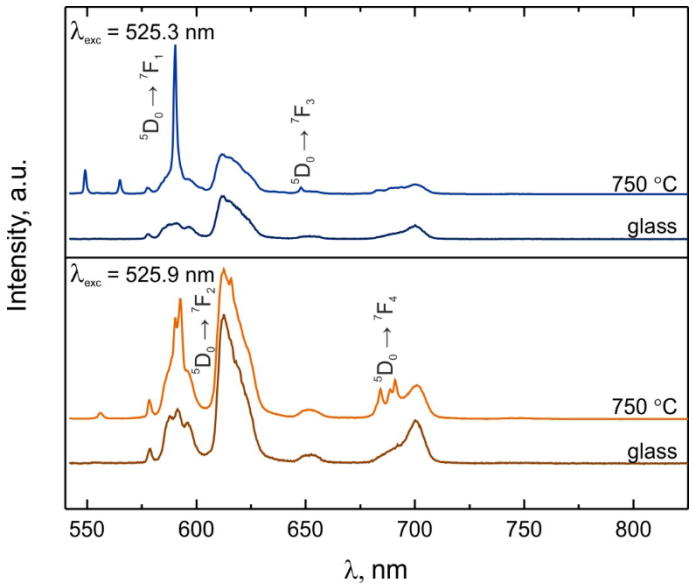

Fig. 4. Low temperature site selective spectra of the S_3 composition glass and glass ceramics annealed at 750 °C. Transitions have been assigned according to [36].

Solid solutions with wide regions of formation can be prepared in CaF_2-REF_3 binary systems [37]. Incorporation of Eu^{3+} in CaF_2 lattice requires heterovalent substitution. Charge compensation can be achieved by either introduction of additional fluorine anions in the structure, which is dominant in dilute solid solutions, or by formation of rare earth ion clusters [38]. When a trivalent impurity substitutes the divalent cation position in the fluorite lattice, excess charge compensators in the vicinity of the impurity modify its local environment. In several site-selective spectroscopy studies of CaF_2:Eu^{3+} single crystals it has been established that the dominant isolated Eu^{3+} ion positions are the cubic and tetragonal centres. The tetragonal distortion in CaF_2 is created by a fluoride interstitial in the next-nearest void position along the [100] direction in respect to Eu^{3+}, while for cubic centres the charge compensation is more distant [36,39–41].

In the glass ceramics we can clearly identify the cubic CaF_2:Eu^{3+} centre excited with 525.3 nm from the narrow single-component luminescence structure of the $^5D_0 \rightarrow {}^7F_1$ transition at 590 nm. The second signal could be attributed to the tetragonal site or Eu^{3+} cluster sites in CaF_2 nanocrystals. Unfortunately, relatively broad luminescence bands of Eu^{3+} in the glass matrix prevent detailed Eu^{3+} site identification in these materials.

3.3. XRD

The introduction of Eu^{3+} in glass did not cause changes in the phase formation; however, as shown in Figure 5, slight XRD peak shift to higher angles with the increase of Eu^{3+} content could be detected suggesting the incorporation of Eu^{3+} in CaF_2 lattice. The substitution of Ca^{2+} by Eu^{3+} results in the increase of CaF_2 lattice parameter and the relation agrees reasonably well with Vegard's law, which states a linear dependence of lattice parameter on the content of substituting compound [42,43].

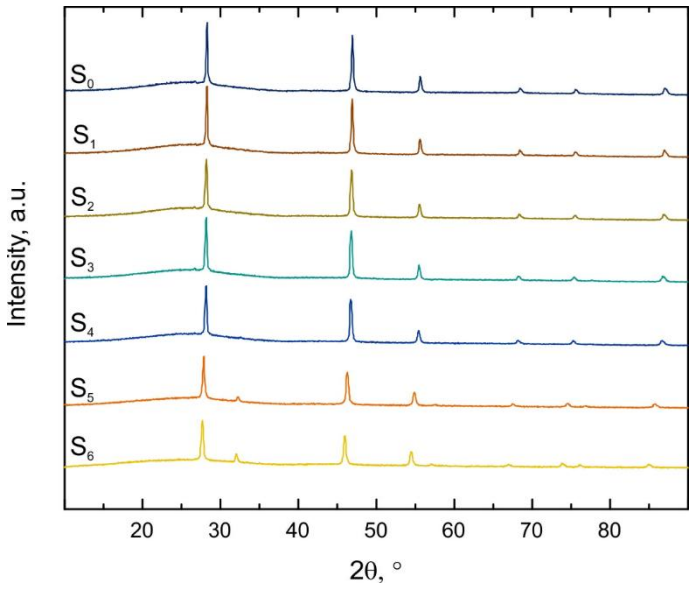

Fig. 5. XRD patterns of glass ceramic samples annealed at 750 °C.

In this research Eu^{3+} content in the CaF_2 nanocrystals was analysed by comparing the lattice parameters of CaF_2:Eu^{3+} nanocrystals in the glass ceramics with polycrystalline CaF_2:Eu^{3+} prepared using hydrothermal synthesis. The results are shown in Figure 6. The lattice parameter of the polycrystalline samples gradually increases with the increase of Eu^{3+} content and it can be fitted with empirical relation reported previously [44]. Slight deviations can be detected for the samples with Eu^{3+} content higher than 20 mol%, which correspond well with the data reported in [43].

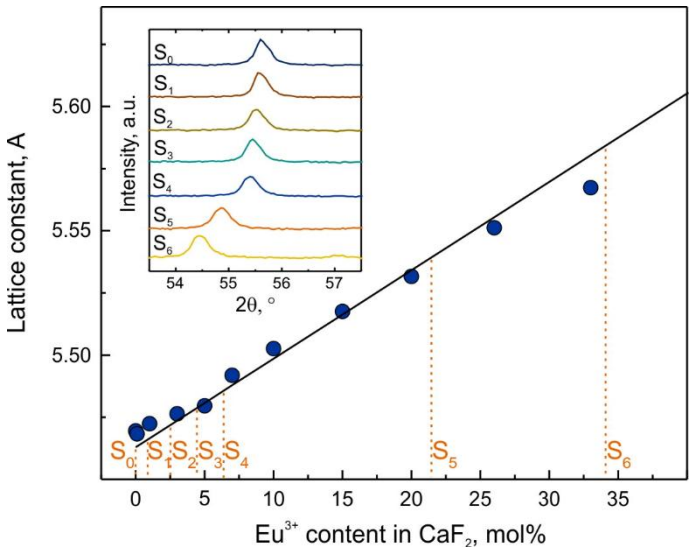

Fig. 6. The change of the lattice constant in CaF_2:Eu^{3+} (solid spheres – experimental points of polycrystalline samples, solid line – empirical relation taken from [41], dashed lines – Eu^{3+} content in CaF_2:Eu^{3+} containing glass ceramics). Inset: XRD pattern of {113} lattice planes of CaF_2: Eu^{3+} in glass ceramics heat treated at 750 °C for 1 h.

The lattice parameter was determined in the glass ceramics and compared with the empiric relation, from which the approximate Eu^{3+} content was estimated. It should be noted that in the glass ceramics slight changes in the lattice parameters could also be associated with the lattice strains in CaF_2 nanocrystals formed during the heat treatment.

3.4. EPR

Direct EPR investigations of Eu^{3+} are of no interest due to the non-degenerate ground state of the ion [35]. Therefore, constant amount of gadolinium was added to all investigated compositions to serve as a paramagnetic probe for EPR purposes. The advantages of Gd^{3+} ions over other paramagnetic impurities are as follows: (1) Gd^{3+} EPR spectra fine structure is sensitive to variations in the local crystal field [45]; (2) EPR spectra are detectable at room temperature; (3) Gd^{3+} incorporates into CaF_2 crystalline phase of oxyfluoride glass ceramics [46]. Furthermore, the addition of gadolinium does not interfere with the visible transmittance of the material because all optical transitions of Gd^{3+} are in the ultraviolet region of electromagnetic spectrum. In the previous studies low concentrations of gadolinium co-dopants have been used to investigate the influence of primary dopant ions on their crystal structure [47–53]. Several effects were observed in the EPR spectra. First, site symmetry of Gd^{3+} centres in CaF_2 and SrF_2 crystals was dependent on the concentration of primary ions [47–49].

Secondly, linewidth of Gd^{3+} EPR transitions was found to increase at higher doping levels [49–53]. In this work we try to establish whether the above-mentioned effects can be exploited to determine Ca:Eu ratio in the crystalline phase of glass ceramics.

EPR spectra of the glass samples showed the typical glass spectrum characteristic to Gd^{3+} ions in disordered environment similar to the previous investigations of gadolinium doped oxyfluoride systems [46,54,55]. The EPR spectrum of $4f^7$ configuration ions (Gd^{3+}, Eu^{2+}) in disordered media is labelled as the "U-type" (from "ubiquitous") and is produced by a broad distribution of second rank zero field splitting (ZFS) parameter values [56,57]. To evaluate the possible contribution of Eu^{2+} ions to the EPR spectra, samples singly doped with europium in analogous composition glass ceramics were investigated. It was determined that the EPR signal intensity arising from Eu^{2+} ions is negligible in comparison to the Gd^{3+} probe signal up to 5 mol% Eu doping. At higher concentration the signals of Gd^{3+} and Eu^{2+} ions in the glass samples are comparable, which for the S_6 sample puts an upper limit of 0.1 mol% Eu^{2+} concentration.

EPR spectra of the S_0 composition samples annealed at different temperatures are shown in figure 7.

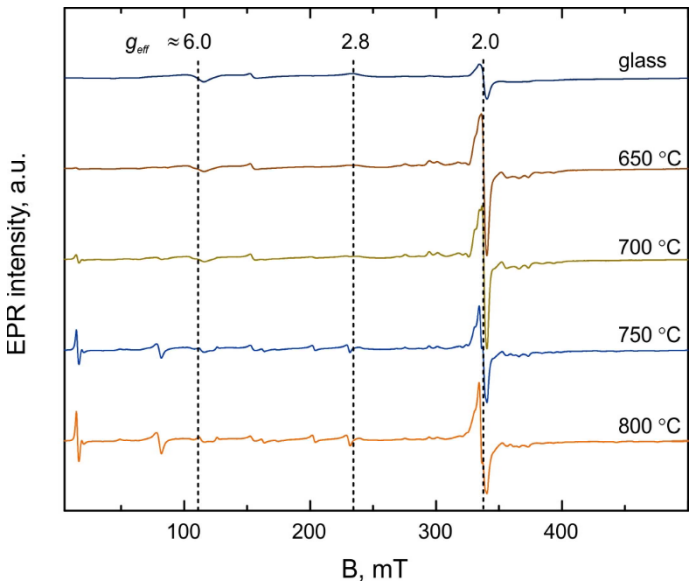

Fig. 7. EPR spectra of S_0 composition samples annealed at different temperatures.

The most prominent features of the "U-type" spectrum at $B \approx 110$ and 230 mT (g_{eff} = 6.0 and 2.8, respectively) remain after the annealing. This means that a part of Gd^{3+} ions resides in the glassy phase. Intense Gd^{3+} EPR signal centred at 330 mT ($g_{eff} \approx 2.0$) overlays the spectrum confirming the

incorporation of the probe in the CaF_2 nanocrystals. For samples annealed at > 700 °C additional set of resonances at $B \approx 15$, 80, 200 and 230 mT can also be observed. The observed signals have been attributed to the cubic (C) and tetragonal (T) $CaF_2:Gd^{3+}$ centres [58], where the symmetry is determined by the direction of charge compensator relative to Gd^{3+}. As has been reported previously in studies of $SrF_2:Gd^{3+}$ polycrystalline systems [59] and glass ceramics containing $CaF_2:Gd^{3+}$ [46], the formation of C and T centres is strongly dependent on the annealing temperature. We observe a rapid increase in T signal intensity in the 650-750 °C sample annealing range, while the additional increase to 800 °C does not have a major effect on T and C centre signal relative intensities. We chose 750 °C as the optimal annealing temperature to avoid undesirable Gd^{3+} signals arising from secondary crystalline phases. Experimental EPR spectra of the glass ceramics annealed at 750 °C are shown in Figure 8.

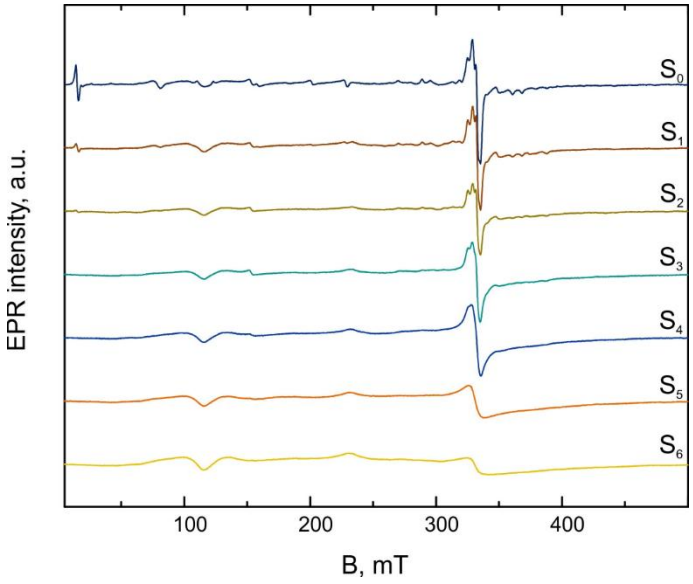

Fig. 8. EPR spectra of glass ceramic samples annealed at 750 °C.

With the increase of Eu^{3+} in the glass ceramics, the relative intensity ratio of tetragonal (T) and cubic (C) centre is decreased. The experimental data imply that for low doping amount the ratio of T/C $CaF_2:Gd^{3+}$ EPR signals could be used to monitor Eu^{3+} content in the crystalline phase of glass ceramics. To test this hypothesis, EPR spectra were investigated for the polycrystalline $CaF_2:Gd^{3+}/Eu^{3+}$ samples. The experimental spectra were fitted using a superposition of two $S = 7/2$ systems with:

- C signal – g = 1.9918, B_4 = 2.33 MHz and spin-Hamiltonian (SH):

$$H = \beta BgS + B_4\ (O_4^0 + 5O_4^4) \quad (1)$$

- T signal – g = 1.992, B_2^0 = -1501.73 MHz, B_4^0 = -1.18 MHz, B_4^4 = -7.59 MHz and SH:

$$H = \beta BgS + B_2^0 O_2^0 + B_4^0 O_4^0 + B_4^4 O_4^4 \quad (2)$$

The symbols in SHs (1) and (2) have their conventional meanings [60]: β – the Bohr magneton; B – the external magnetic field value; g – the spectroscopic splitting factor; B_k^q – ZFS parameters and O_k^q – Steven operator equivalents, where k = 2, 4, 6 and q = +k, …., -k.

Afterwards, signal amplitudes were calculated from EasySpin "Weight" function. The "Weight" of signal T relative to signal C was defined as the T/C ratio parameter. T/C as a function of Eu^{3+} doping in CaF_2 polycrystals is shown in Figure 9. The uncertainties for the polycrystalline samples have been determined as ± 15 % based on the repeatability of synthesis of 0 mol% and 1 mol% Eu concentration samples. The dashed lines indicate the values of T/C and the respective Eu^{3+} content in CaF_2 nanocrystals for the glass ceramic samples. An example of simulated signals is given in the inset of Figure 9.

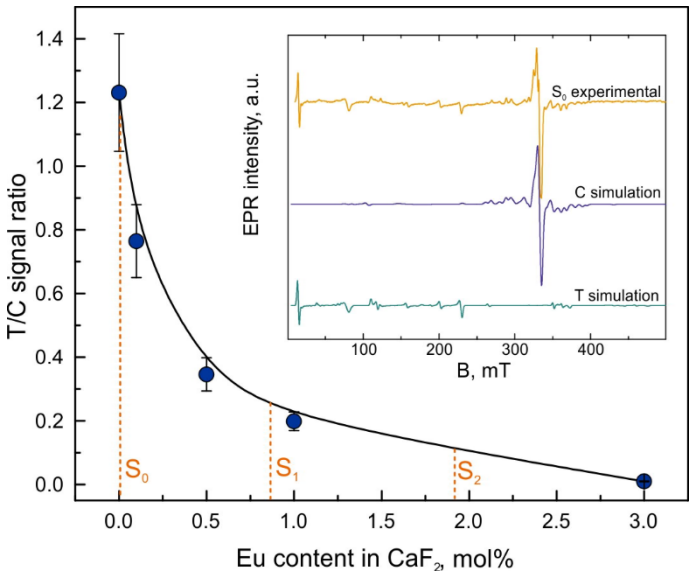

Fig. 9. T/C ratio as a function of Eu^{3+} doping in CaF_2 polycrystals. Dashed lines indicate the determined values of Eu^{3+} content in glass ceramics. Inset shows the experimental spectrum of the S_0 sample and the simulated components of T and C signals.

The fitted values of SH parameters for the T and C centres are in line with the previous studies of Gd^{3+} in CaF_2 single crystals [58]. The T signal is not observed in polycrystalline CaF_2 if Eu^{3+} doping exceeds 3 mol%. The C signal remains but it is significantly broadened. Several factors could contribute to this phenomenon such as variations in ZFS parameter values and linewidth increase of ZFS transitions themselves. We assume that the formation of isolated CaF_2:Gd^{3+} centres is hindered by the introduction of additional impurities and the line broadening in the glass ceramics is caused by the formation of Eu^{3+}-F^- dipole and Eu^{3+} clusters. Similar effects have been observed in gadolinium doped fluorite single crystals for large concentrations of RE^{3+} ions [49,50,52,53].

To quantify this effect, 310-350 mT spectra region containing the most prominent CaF_2:Gd^{3+} line was selected and the variation in its linewidth as a function of Eu^{3+} concentration in CaF_2 was investigated. EPR resonance lines are typically described by either Lorentzian or Gaussian type functions – the former is used to characterize lineshapes determined by the relaxation processes, while the latter is used to describe resonances broadened by multiple overlapping components [61]. As the EPR spectra of glass ceramics are effectively composed of a superposition of a glass background signal and myriad orientation-dependent single crystal spectra, it is more reasonable to fit our spectra with a Gaussian function. The linewidth of the C signal as a function of Eu^{3+} content in CaF_2 is shown in Figure 10. An example of the simulations is given in the inset of Figure 10. The uncertainties for the polycrystalline samples have been determined based on the repeatability of synthesis of 0 mol% and 1 mol% Eu concentration samples.

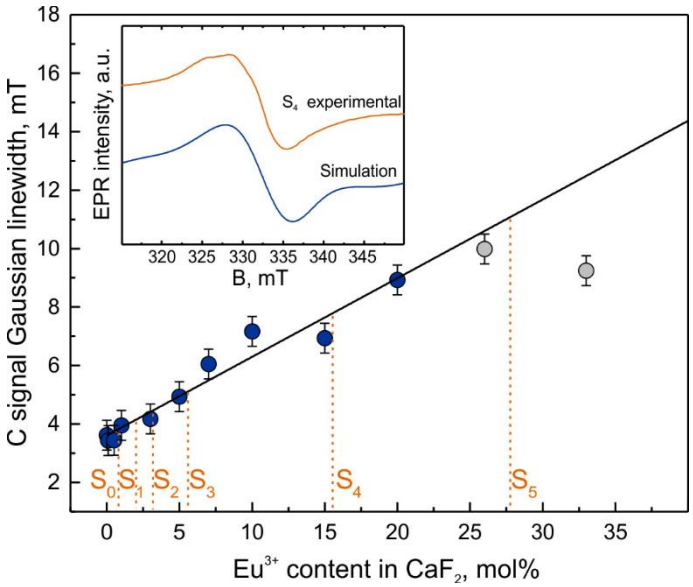

Fig. 10. C signal linewidth as a function of Eu^{3+} doping in CaF_2 polycrystals. Dashed lines indicate the determined values of Eu^{3+} content in glass ceramics. Inset shows the experimental and simulated spectra of the S_4 sample.

Up to 20 mol% Eu^{3+} doping the linewidth of Gd^{3+} EPR spectra can be approximated with a straight line; for larger Eu^{3+} content linewidth saturation effects are observed. We use the linear dependence region to evaluate activator distribution in the glass ceramics. The results of EPR and XRD investigations are presented in Table 3. For the EPR data the error estimates have been made based on the uncertainties of calibration curves presented in Figures 9 and 10. For the XRD results the credibility of results is estimated to be ± 10 %.

Table 3

Sample	Eu content in CaF_2 nanocrystals, mol%		
	XRD	EPR	
		T/C signal ratio	C signal linewidth
S_0	0.0	0.0	0.0
S_1	0.9 ± 0.1	0.9 ± 0.3	0.7 ± 0.5
S_2	2.4 ± 0.2	1.9 ± 0.5	1.9 ± 0.5
S_3	4.6 ± 0.5	> 3.0	4.1 ± 0.8
S_4	6.3 ± 0.6		10.9 ± 1.4
S_5	21.5 ± 2.2		> 20.0
S_6	33.9 ± 3.4		

For low activator concentrations the analysis of Gd^{3+} probe EPR spectra yields consistent results with dopant-induced lattice constant changes determined from XRD. The T/C approach is limited by the requirement of having several available site positions for paramagnetic ions in the crystal. Primary dopant distribution determination based on EPR probe linewidth simulations is more straightforward

and could be applied to a larger variety of systems. In our case, however, Eu^{3+} content in CaF_2 is overestimated for the glass ceramic samples S_4-S_6. The increased line broadening in the glass ceramics could be attributed to Eu^{2+} ions possibly residing in the glass matrix and should be investigated in more detail. Additionally, the effects of the nano-size nature of crystals have been found to result in the broadening of EPR spectra in SrF_2:Gd^{3+} [59] and LaF_3:Gd^{3+} [62] nanoparticles. To minimize these effects on quantitative analysis performed here, the investigations were carried out for the glass ceramics annealed at 750 °C, where the average CaF_2 crystal size exceeded 40 nm. Another factor, which should be taken into account, is that at large RE doping Gd^{3+} itself becomes a "non-innocent" probe and participates in the formation of Gd-RE ion pairs and clusters [50]. The approach based on the isolated centre EPR spectra simulations could be justified by the fact that the defect formation in the glass ceramics was compared to the polycrystalline CaF_2.

To summarize, a novel methodology for assessing activator distribution in glass ceramics is proposed based on activator-induced changes on Gd^{3+} probe EPR spectra. The results obtained with this approach are sound with the results of XRD analysis. We can conclude that EPR spectroscopy can be used for the quantitative analysis of RE content in the crystalline phase of glass ceramics. In this respect, the proposed method is an excellent alternative for the investigation of materials in cases when typical methods cannot be applied, such as crystals with similar activator and host matrix ionic radii implying insignificant changes of lattice parameters. Nevertheless, the multiple factors, which influence the spectroscopic properties of RE ions in nanocomposite systems, should be investigated in more detail. When activator distribution in composite materials is estimated, a combination of several methods is highly recommended.

4. Conclusions

In this study a novel approach for the analysis of activator distribution in nanocrystalline glass ceramics has been demonstrated. XRD and EPR techniques have been combined to investigate Eu^{3+} incorporation efficiency in CaF_2 crystalline phase of oxyfluoride glass ceramics. The linear dependence of CaF_2 lattice parameter on Eu^{3+} dopant concentration has been used to determine the distribution of activators in glass ceramics. For the investigations of non-magnetic Eu^{3+} ions via EPR

spectroscopy, paramagnetic probe ions can be introduced to glass ceramics. Gd^{3+} probe local structure is modified by the addition of Eu^{3+} in CaF_2. At low concentration range of europium, the ratio of tetragonal-to-cubic CaF_2:Gd^{3+} EPR signals proved to be more sensitive towards changes of the concentration, while at higher concentrations of europium the broadening of the spectrum seems to be more appropriate for the evaluation of Eu^{3+} content. Both effects can be applied to evaluate the content of Eu^{3+} in the nanocrystals present in glass ceramics and up to 5 mol% are in a good agreement with the estimations from XRD.

Acknowledgements.

The authors are grateful to Dr. Andris Fedotovs for photography of the samples. This research is funded by the Latvian Council of Science, project "Novel transparent nanocomposite oxyfluoride materials for optical applications", project No. LZP-2018/1-0335.

References

[1] P. Cortelletti, M. Pedroni, F. Boschi, S. Pin, P. Ghigna, P. Canton, F. Vetrone, A. Speghini, Luminescence of Eu^{3+} activated CaF_2 and SrF_2 nanoparticles: effect of the particle size and co-doping with alkaline ions, Cryst. Growth Des. 18 (2018) 686–694. doi:10.1021/acs.cgd.7b01050.

[2] F.A. Modine, D. Lubben, J.B. Bates, Electrical conduction in CaF_2 and CaF_2-Al_2O_3 nanocomposite films on Al_2O_3 substrates, J. Appl. Phys. 74 (1993) 2658–2664. doi:10.1063/1.354657.

[3] G. Hu, Y. Sun, S. Wu, W. Li, C. Hu, J. Zhuang, X. Zhang, B. Lei, Y. Liu, Assembly of shell/core CDs@CaF_2 nanocomposites to endow polymer with multifunctional properties, Nanotechnology. 30 (2019). doi:10.1088/1361-6528/aafcd4.

[4] G.A. Kumar, C.W. Chen, R. Riman, S. Chen, D. Smith, J. Ballato, Optical properties of a transparent CaF_2:Er^{3+} fluoropolymer nanocomposite, Appl. Phys. Lett. 86 (2005) 10–13. doi:10.1063/1.1947891.

[5] L. Song, J. Gao, M. Liang, X. Li, J. Li, L. Wang, Preparation and luminescent properties of CaF_2:Ln^{3+} (Ln:Er, Er/Yb)/Nafion composite films, J. Rare Earths. 37 (2019) 232–236. doi:10.1016/j.jre.2018.05.020.

[6] X. Liu, W. Di, W. Qin, Cooperative luminescence mediated near infrared photocatalysis of CaF_2:Yb@$BiVO_4$ composites, Appl. Catal. B Environ. 205 (2017) 158–164. doi:10.1016/j.apcatb.2016.12.027.

[7] K. Shinozaki, A. Noji, T. Honma, T. Komatsu, Morphology and photoluminescence properties of Er^{3+}-doped CaF_2 nanocrystals patterned by laser irradiation in oxyfluoride glasses, J. Fluor. Chem. 145 (2013) 81–87. doi:10.1016/j.jfluchem.2012.10.007.

[8] P.P. Fedorov, A.A. Luginina, A.I. Popov, Transparent oxyfluoride glass ceramics, J. Fluor. Chem. 172 (2015) 22–50. doi:10.1016/j.jfluchem.2015.01.009.

[9] P.P. Fedorov, A.A. Luginina, S. V. Kuznetsov, V. V. Osiko, Nanofluorides, J. Fluor. Chem. 132 (2011) 1012–1039. doi:10.1016/j.jfluchem.2011.06.025.

[10] C. Struebing, J.Y. Chong, G. Lee, M. Zavala, A. Erickson, Y. Ding, C.L. Wang, Y. Diawara, R. Engels, B. Wagner, Z. Kang, A neutron scintillator based on transparent nanocrystalline CaF_2:Eu glass ceramic, Appl. Phys. Lett. 108 (2016). doi:10.1063/1.4945999.

[11] J. Fu, J.M. Parker, P.S. Flower, R.M. Brown, Eu^{2+} ions and CaF_2 -containing transparent glass-ceramics, Mater. Res. Bull. 37 (2002) 1843–1849.

[12] Y. Jiang, P. Zhang, T. Wei, J. Fan, B. Jiang, X. Mao, L. Zhang, Europium doped transparent glass ceramics containing CaF_2 micron-sized crystals: Structural and optical characterization, RSC Adv. 60 (2016) 55366–55373. doi:10.1039/C6RA10288C.

[13] Q. Xusheng, L.U.O. Qun, F.A.N. Xianping, W. Minquan, Local vibration around rare earth ions in alkaline earth fluorosilicate transparent glass and glass ceramics using Eu^{3+} probe, J. Rare Earths. 26 (2008) 883–888. doi:10.1016/S1002-0721(09)60026-0.

[14] M. Itoh, T. Sakurai, T. Yamakami, J. Fu, Time-resolved luminescence study of CaF_2:Eu^{2+} nanocrystals in glass-ceramics, J. Lumin. 112 (2005) 161–165. doi:10.1016/j.jlumin.2004.09.017.

[15] M. Secu, C.E. Secu, S. Polosan, G. Aldica, C. Ghica, Crystallization and spectroscopic properties of Eu-doped CaF_2 nanocrystals in transparent oxyfluoride glass-ceramics, J. Non. Cryst. Solids. 355 (2009) 1869–1872. doi:10.1016/j.jnoncrysol.2009.04.062.

[16] M. Secu, C.E. Secu, C. Ghica, Eu^{3+}-doped CaF_2 nanocrystals in sol–gel derived glass–ceramics, Opt. Mater. (Amst). 33 (2011) 613–617. doi:10.1016/j.optmat.2010.11.016.

[17] A.C. Galca, N. Preda, C.E. Secu, C.R. Luculescu, M. Secu, Spectroscopic ellipsometry investigations of Eu-doped oxy-fluoride glass and glass-ceramics, Opt. Mater. (Amst). 34 (2012) 1493–1496. doi:10.1016/j.optmat.2012.03.015.

[18] L. Yanhong, Z. Li, Z. Yongming, M. Jing, Preparation and luminescence properties of Eu^{3+} doped oxyfluoride borosilicate glass ceramics, J. Rare Earths. 30 (2012) 1195–1198. doi:10.1016/S1002-0721(12)60204-X.

[19] W. Deng, J. Cheng, New transparent glass – ceramics containing large grain Eu^{3+}:CaF_2 nanocrystals, Mater. Lett. 73 (2012) 112–114. doi:10.1016/j.matlet.2012.01.016.

[20] A.V. Egorysheva, A.P. Melekhov, V.D. Volodin, I.A. Gerasimov, T.B. Kuvshinova, G.S. Bogdanov, I.P. Sipailo, T.D. Dudkina, D.V. Lavrukhin, Preparation of Transparent Oxyfluoroborate Glass-Ceramics Containing CaF_2⟨Eu⟩ Crystals, Inorg. Mater. 49 (2013) 1144–1148. doi:10.1134/S0020168513100026.

[21] F. Hu, Z. Zhao, F. Chi, X. Wei, M. Yin, Structural characterization and temperature-dependent luminescence of CaF_2:Tb^{3+}/Eu^{3+} glass ceramics, J. Rare Earths. 35 (2017) 536–541. doi:10.1016/S1002-0721(17)60945-1.

[22] C. Zhu, D. Wu, Y. Zhang, M. Zhang, Y. Yue, Composition dependence of the optical and structural properties of Eu-doped oxyfluoride glasses, J. Alloys Compd. 632 (2015) 291–295. doi:10.1016/j.jallcom.2015.01.207.

[23] G. Krieke, A. Sarakovskis, M. Springis, Ordering of fluorite-type phases in erbium-doped oxyfluoride glass ceramics, J. Eur. Ceram. Soc. 38 (2018) 235–243. doi:10.1016/j.jeurceramsoc.2017.08.037.

[24] X. Qiao, X. Fan, M. Wang, X. Zhang, Spectroscopic properties of Er^{3+} and Yb^{3+} co-doped glass

ceramics containing SrF_2 nanocrystals, J. Phys. D. Appl. Phys. 42 (2009) 055103. doi:10.1088/0022-3727/42/5/055103.

[25] X. Qiao, X. Fan, Z. Xue, X. Xu, Q. Luo, Intense ultraviolet upconversion luminescence of Yb^{3+} and Tb^{3+} co-doped glass ceramics containing SrF_2 nanocrystals, J. Lumin. 131 (2011) 2036–2041. doi:10.1016/j.jlumin.2011.05.012.

[26] G. Krieke, A. Sarakovskis, M. Springis, Cubic and rhombohedral $Ba_4Lu_3F_{17}$:Er^{3+} in transparent glass ceramics: Crystallization and upconversion luminescence, J. Lumin. 200 (2018) 265–273. doi:10.1016/j.jlumin.2018.04.016.

[27] J.I. Langford, A.J.C. Wilson, Scherrer after sixty years: A survey and some new results in the determination of crystallite size, J. Appl. Crystallogr. 11 (1978) 102–113. doi:10.1107/S0021889878012844.

[28] A. Boultif, D. Loueer, Indexing of powder diffraction patterns for low-symmetry lattices by the successive dichotomy method, J. Appl. Crystallogr. (1991). doi:10.1107/S0021889891006441.

[29] D. Louër, A. Boultif, Powder pattern indexing and the dichotomy algorithm, in: Zeitschrift Fur Krist. Suppl., 2007.

[30] S. Stoll, A. Schweiger, EasySpin, a comprehensive software package for spectral simulation and analysis in EPR, J. Magn. Reson. 178 (2006) 42–55.

[31] Z. Lin, H. Zeng, Y. Yang, X. Liang, G. Chen, L. Sun, The effect of fluorine anions on the luminescent properties of Eu-Doped oxyfluoride aluminosilicate glasses, J. Am. Ceram. Soc. 93 (2010) 3095–3098. doi:10.1111/j.1551-2916.2010.04067.x.

[32] A. Antuzevics, M. Kemere, G. Krieke, R. Ignatans, Electron paramagnetic resonance and photoluminescence investigation of europium local structure in oxyfluoride glass ceramics containing SrF_2 nanocrystals, Opt. Mater. (Amst). 72 (2017) 749–755. doi:10.1016/j.optmat.2017.07.024.

[33] R. Scheps, Ultraviolet-to-Visible Luminescent Conversion in CaF_2:Eu^{2+} and SrF_2:Eu^{2+} Crystals, J. Electrochem. Soc. 136 (1989) 9–11.

[34] G.N. Chapman, A.J. Walton, Triboluminescence of fluorites, J. Phys. C Solid State Phys. 16 (1983) 5543–5551. doi:10.1088/0022-3719/16/28/021.

[35] K. Binnemans, Interpretation of europium(III) spectra, Coord. Chem. Rev. 295 (2015) 1–45. doi:10.1016/j.ccr.2015.02.015.

[36] R.J. Hamers, J.R. Wietfeldt, J.C. Wright, Defect chemistry in CaF_2:Eu^{3+}, J. Chem. Phys. 77 (1982) 683–692. doi:10.1063/1.443882.

[37] P.P. Fedorov, B.P. Sobolev, Phase diagrams of the CaF_2-(Y,Ln) F_3 systems II. A discussion, J. Less Common Met. 63 (1979) 31–43. doi:https://doi.org/10.1016/0022-5088(79)90206-6.

[38] P.P. Fedorov, Association of point defects in non-stoichiometric $M_{1-x}R_xF_{2+x}$ fluorite-type solid solutions, Butll. Soc. Cat. Cien. XII (1991) 349–381.

[39] K.M. Cirillo-Penn, J.C. Wright, Laser spectroscopic measurement of point-defect dynamics in Eu^{3+}:CaF_2, Phys. Rev. B. 41 (1990) 10799–10807.

[40] L.R. Olsen, A.O. Wright, J.C. Wright, Localized fluoride diffusion and defect equilibrium in CaF_2:Eu^{3+} using site-selective spectroscopy and high-pressure techniques, Phys. Rev. B. 53 (1996) 135–144.

[41] J.-P.R. Wells, R.J. Reeves, Polarized laser selective excitation and Zeeman infrared absorption of C_{4v} and C_{3v} symmetry centers in Eu^{3+}-doped CaF_2, SrF_2 and BaF_2 crystals, Phys. Rev. B. 64 (2001) 1–10. doi:10.1103/PhysRevB.64.035102.

[42] A. R. Denton and N. W. Ashcroft, Vegard's law, Phys. Rev. A. 43 (1991) 3161–3164. doi:10.1103/PhysRevA.43.3161.

[43] P.P. Fedorov, B.P. Sobolev, Concentration dependence of unit-cell parameters of phases $M_{1-x}R_xF_{2+x}$ with the fluorite structure, Sov. Phys. Crystallogr. 37 (1992) 651–656.

[44] O. Greis, M. Kieser, Darstellung und Eigenschaften der festen Lösungen $(Ca,SE)F_{2,33}$ mit SE = Y, La, Ln und der korrespondierenden Ordnungsphasen Ca_2SEF_7 mit SE = Er – Lu und Y, ZAAC - J. Inorg. Gen. Chem. 479 (1981) 165–170. doi:10.1002/zaac.19814790820.

[45] H.A. Buckmaster, Y.H. Shing, A survey of the EPR spectra of Gd^{3+} in single crystals, Phys. Status Solidi. 12 (1972) 325–361. doi:10.1002/pssa.2210120202.

[46] A. Fedotovs, A. Antuzevics, U. Rogulis, M. Kemere, R. Ignatans, Electron paramagnetic resonance and magnetic circular dichroism of Gd^{3+} ions in oxyfluoride glass–ceramics containing CaF_2 nanocrystals, J. Non. Cryst. Solids. 429 (2015) 118–121. doi:10.1016/j.jnoncrysol.2015.08.036.

[47] G.K. Miner, T.P. Graham, G.T. Johnston, Effect of a Ce^{3+} Codopant on the Gd^{3+} EPR Spectrum of SrF_2 at Room Temperature, J. Chem. Phys. 57 (1972) 1263–1270. doi:10.1063/1.1678385.

[48] E. Laredo, M. Diaz, N. Suarez, A. Bello, Paramagnetic centers and dipolar defects in CaF_2:Gd^{3+} and CaF_2:Gd^{3+}+Lu^{3+}, Phys. Rev. B. 46 (1992) 11415–11424.

[49] H.W. Den Hartog, Defect structure and defect-defect interactions in solid solutions of AF_2 and RF_3 doped with Gd^{3+} probes, Phys. Rev. B. 27 (1983) 20–26.

[50] A.B. Arauzo, R. Alcala, P.J. Alonso, Pulsed EPR Spectroscopy of Gd^{3+} Centers in $Ca_{1-x}R_xF_{2+x}$ (R=La, Y) Mixed Crystals, Appl. Magn. Reson. 12 (1997) 375–387.

[51] H.W. Den Hartog, K.F. Pen, J. Meuldijk, Defect structure and charge transport in solid solutions $Ba_{1-x}La_xF_{2+x}$, Phys. Rev. B. 28 (1983) 6031–6040.

[52] R. Alcala, P.J. Alonso, B. Sobolev, Electron paramagnetic resonance and luminescence of Gd^{3+} in the mixed fluorides $Ca_{1-x}La_xF_{2+x}$ and $Ca_{1-x}Y_xF_{2+x}$, Radiat. Eff. Defects Solids Inc. Plasma Sci. Plasma Technol. 119–121 (1991) 243–248. doi:10.1080/10420159108224883.

[53] E. Laredo, N. Suarez, A. Bello, M. Puma, Clustering of Y^{3+} in BaF_2 using Gd^{3+} as paramagnetic probes, Solid State Ionics. 37 (1990) 103–113. doi:10.1016/0167-2738(90)90233-H.

[54] A. Antuzevics, M. Kemere, R. Ignatans, Local structure of gadolinium in oxyfluoride glass matrices containing SrF_2 and BaF_2 crystallites, J. Non. Cryst. Solids. 449 (2016) 29–33. doi:10.1016/j.jnoncrysol.2016.07.015.

[55] A. Antuzevics, U. Rogulis, A. Fedotovs, A.I.I. Popov, Crystalline phase detection in glass ceramics by EPR spectroscopy, Low Temp. Phys. 44 (2018) 449–454. doi:10.1063/1.5030462.

[56] C.M. Brodbeck, L.E. Iton, The EPR spectra of Gd^{3+} and Eu^{2+} in glassy systems, J. Chem. Phys. 83 (1985) 4285. doi:10.1063/1.449041.

[57] C. Legein, J.Y. Buzaré, G. Silly, C. Jacoboni, The local field distribution of Gd^{3+} in transition metal fluoride glasses investigated by electron paramagnetic resonance, J. Phys. Condens.

Matter. 8 (1996) 4339–4350. doi:10.1088/0953-8984/8/23/023.

[58] S.A. Al'tshulter, B.M. Kozyrev, Electron Paramagnetic Resonance in Compounds of Transition Elements, Wiley, 1974.

[59] A. Antuzevics, M. Kemere, G. Krieke, Multisite formation in gadolinium doped SrF_2 nanoparticles, J. Alloys Compd. 762 (2018) 500–507. doi:10.1016/j.jallcom.2018.05.283.

[60] A. Abragam, B. Bleaney, Electron Paramagnetic Resonance of Transition Ions, in: Electron Paramagn. Reson. Transit. Ions, Clarendon Press, 1970. doi:10.1017/CBO9781107415324.004.

[61] J.A. Weil, J.R. Bolton, Electron Paramagnetic Resonance, Wiley, 2007.

[62] A.M. Gazizulina, E.M. Alakshin, E.I. Baibekov, R.R. Gazizulin, M.Y. Zakharov, A. V. Klochkov, S.L. Korableva, M.S. Tagirov, Electron paramagnetic resonance of Gd^{3+} ions in powders of LaF_3:Gd^{3+} nanocrystals, JETP Lett. 99 (2014) 149–152. doi:10.1134/S0021364014030084.

Institute of Solid State Physics, University of Latvia as the Center of Excellence has received funding from the European Union's Horizon 2020 Framework Programme H2020-WIDESPREAD-01-2016-2017-TeamingPhase2 under grant agreement No. 739508, project CAMART²

Figure captions

Fig. 1. XRD patterns of S_3 composition samples annealed at different temperatures.

Fig. 2. a) Photograph of S_3 glass and glass ceramics heat treated at 700 °C for 1 h and SEM micrographs of S_3 glass ceramics heat treated at b) 700 °C, c) 750 °C and d) 800 °C for 1h.

Fig. 3. Intensity of room temperature Eu^{3+} photoluminescence for glass ceramics annealed at 750 °C. Inset shows the photoluminescence spectrum of the S_3 composition sample.

Fig. 4. Low temperature site selective spectra of the S_3 composition glass and glass ceramics annealed at 750 °C. Transitions have been assigned according to [36].

Fig. 5. XRD patterns of glass ceramic samples annealed at 750 °C.

Fig. 6. The change of the lattice constant in CaF_2:Eu^{3+} (solid spheres – experimental points of polycrystalline samples, solid line – empirical relation taken from [41], dashed lines – Eu^{3+} content in CaF_2:Eu^{3+} containing glass ceramics). Inset: XRD pattern of {113} lattice planes of CaF_2: Eu^{3+} in glass ceramics heat treated at 750 °C for 1 h.

Fig. 7. EPR spectra of S_0 composition samples annealed at different temperatures.

Fig. 8. EPR spectra of glass ceramic samples annealed at 750 °C.

Fig. 9. T/C ratio as a function of Eu^{3+} doping in CaF_2 polycrystals. Dashed lines indicate the determined values of Eu^{3+} content in glass ceramics. Inset shows the experimental spectrum of the S_0 sample and the simulated components of T and C signals.

Fig. 10. C signal linewidth as a function of Eu^{3+} doping in CaF_2 polycrystals. Dashed lines indicate the determined values of Eu^{3+} content in glass ceramics. Inset shows the experimental and simulated spectra of the S_4 sample.

Figure 1

Click here to download high resolution image

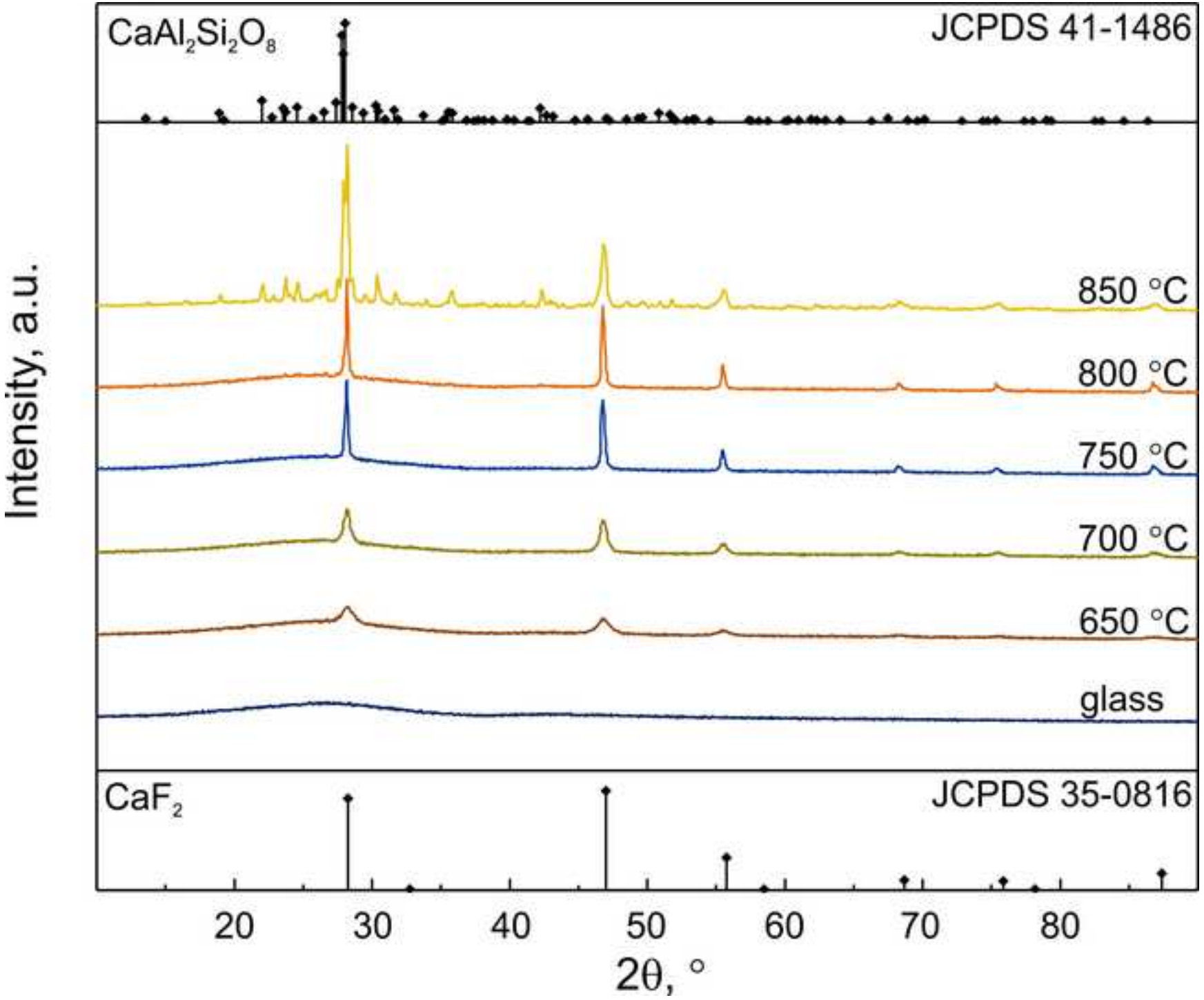

Figure 2

Click here to download high resolution image

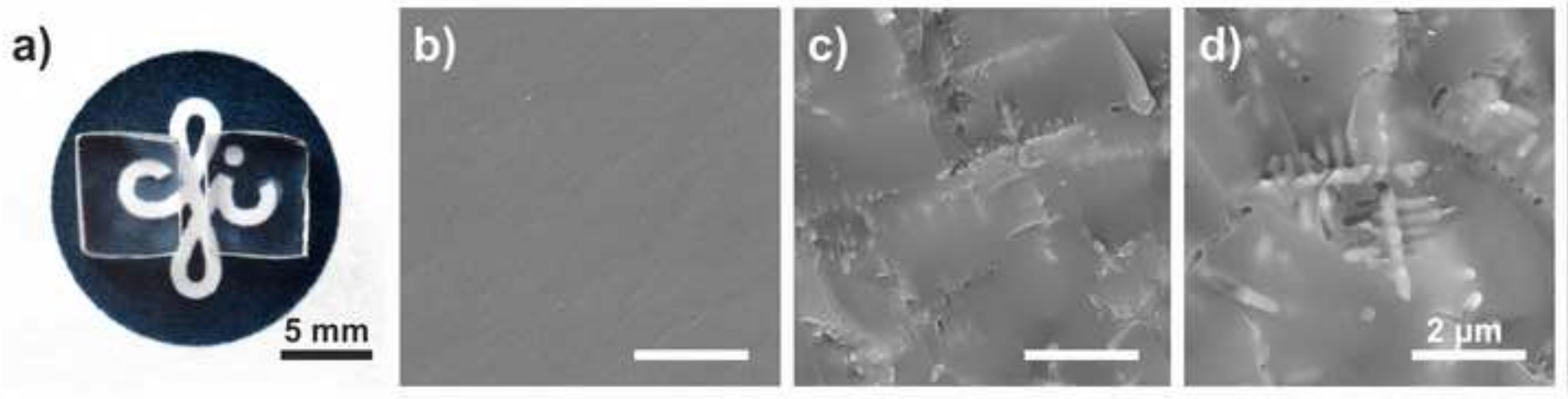

Figure 3

Click here to download high resolution image

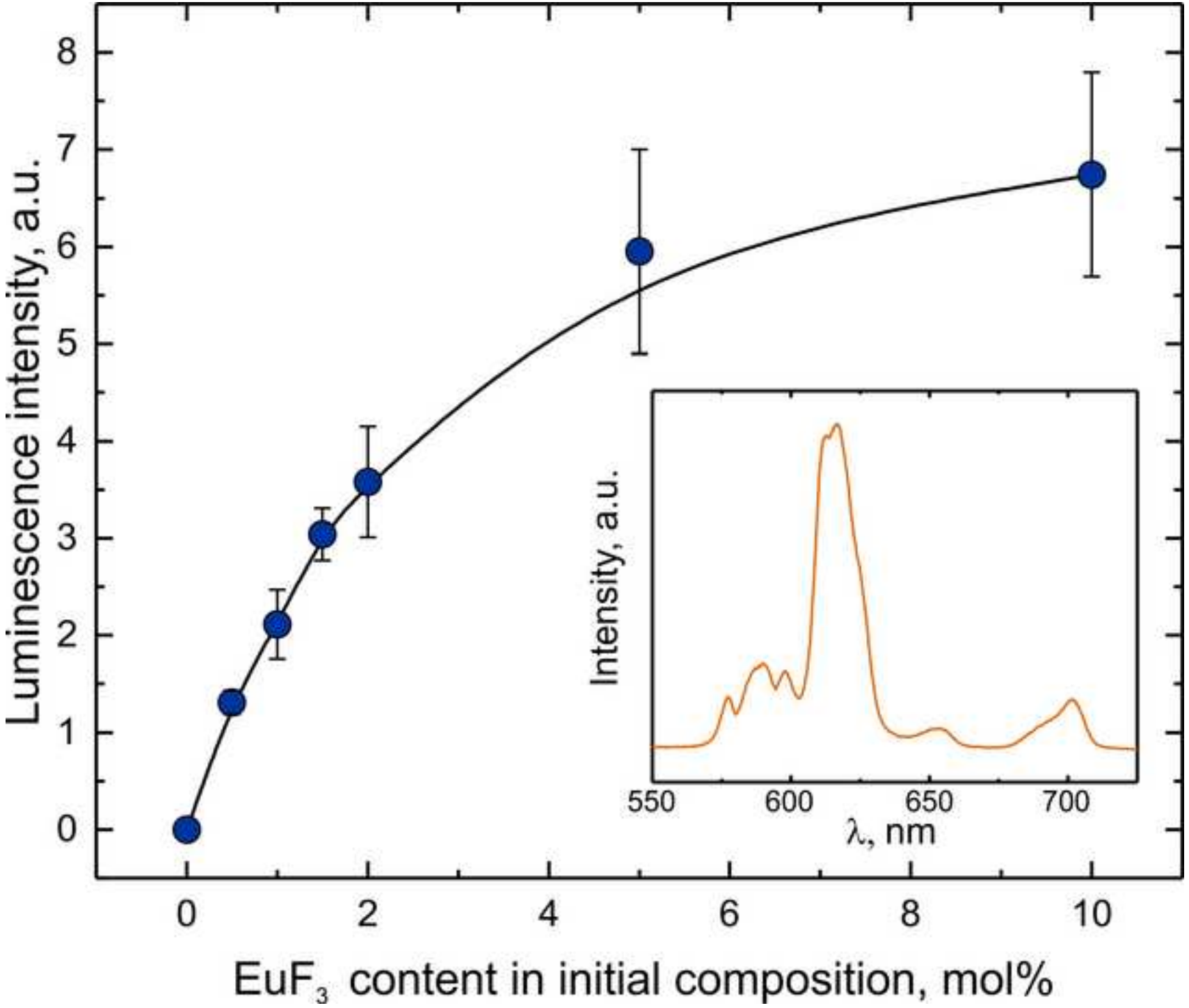

Figure 4

Click here to download high resolution image

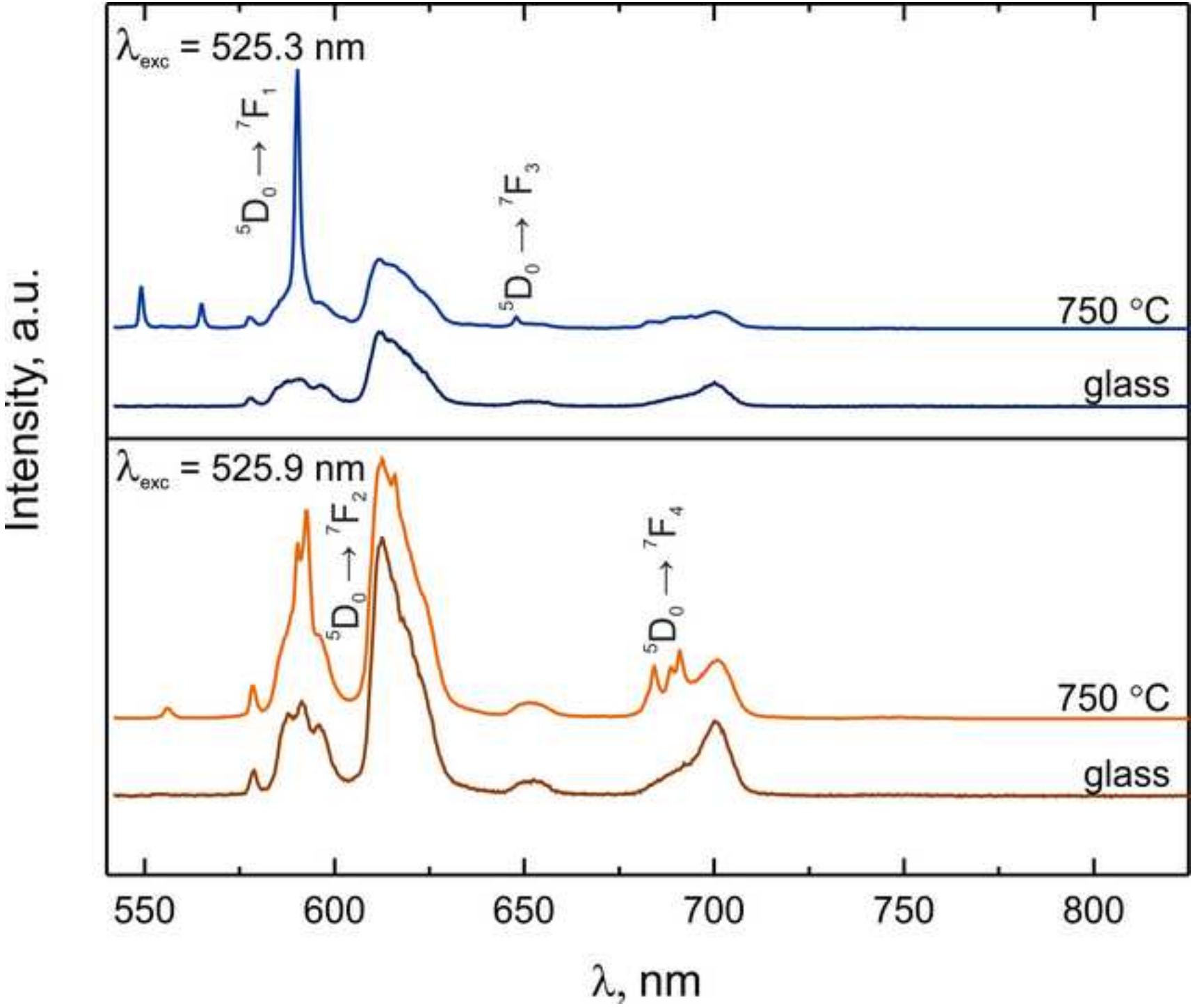

Figure 5

Click here to download high resolution image

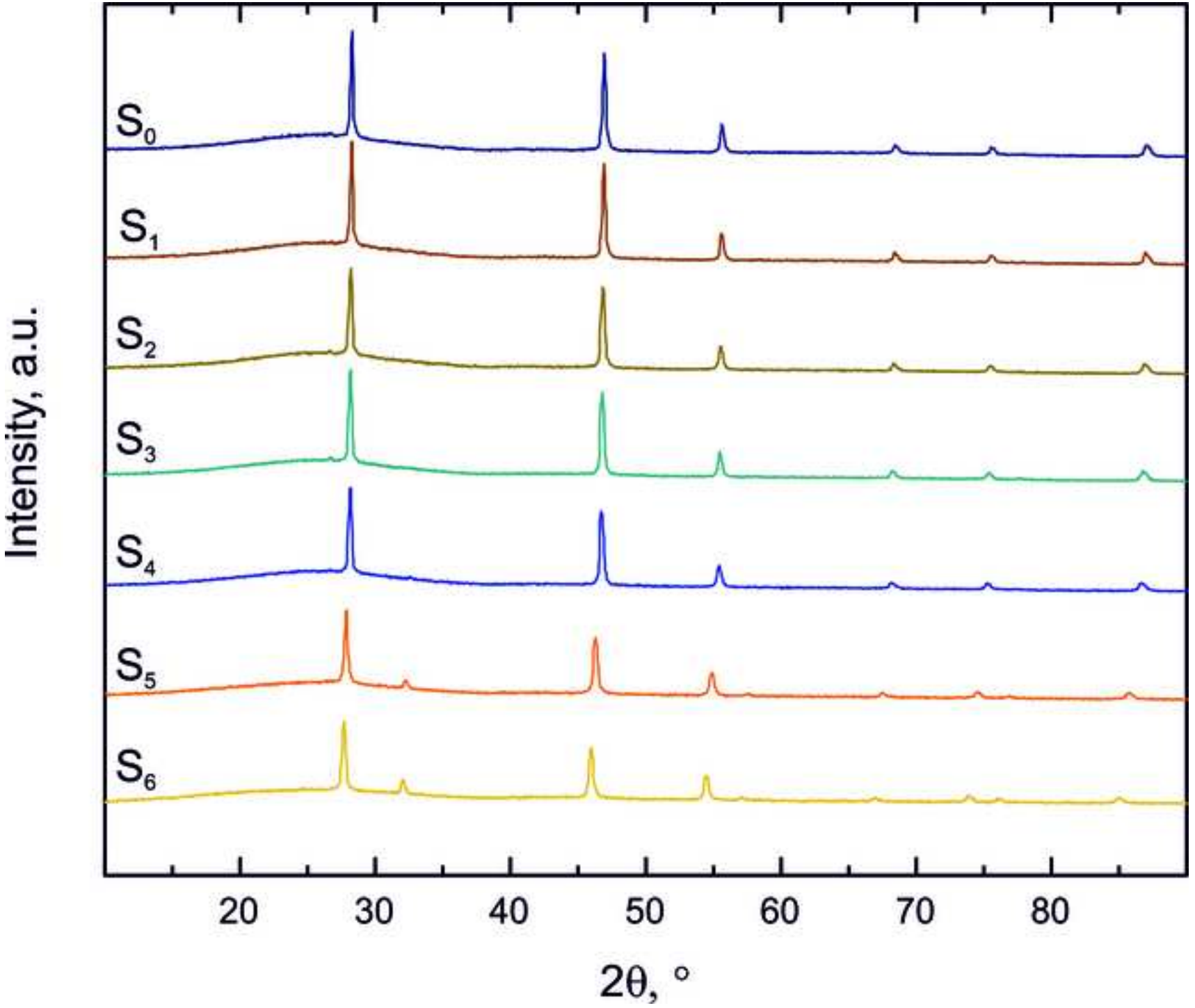

Figure 6

Click here to download high resolution image

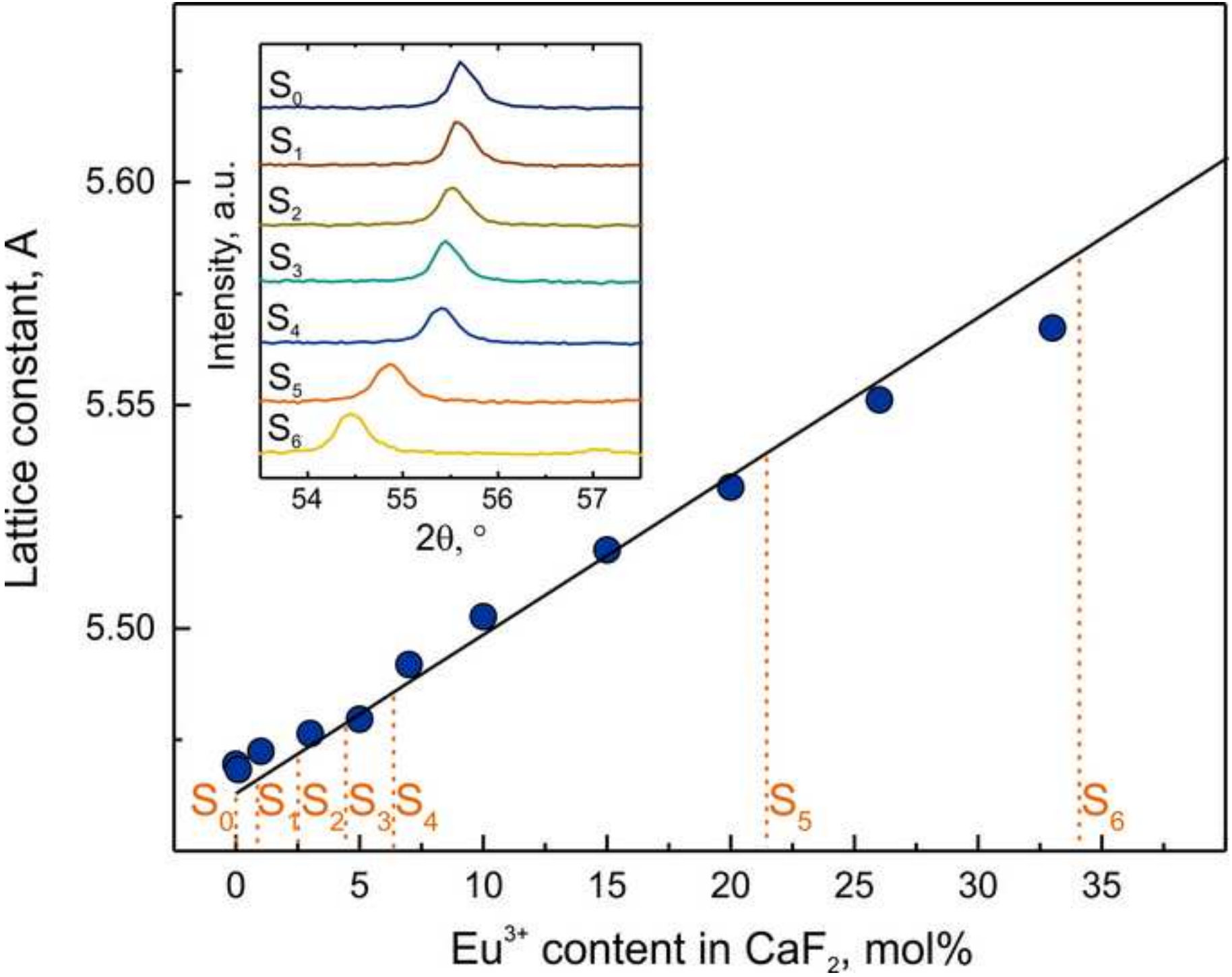

Figure 7

Click here to download high resolution image

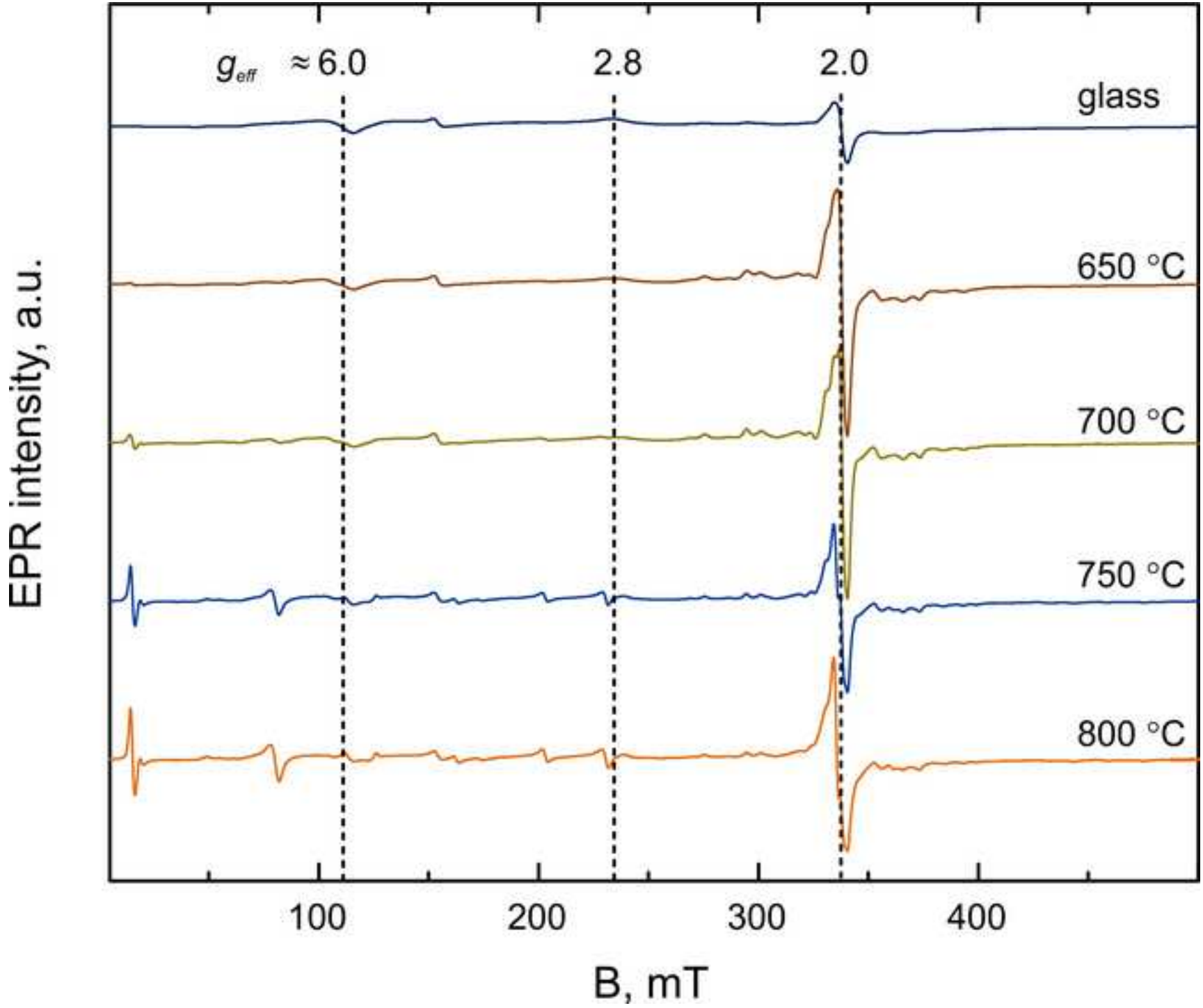

Figure 8

Click here to download high resolution image

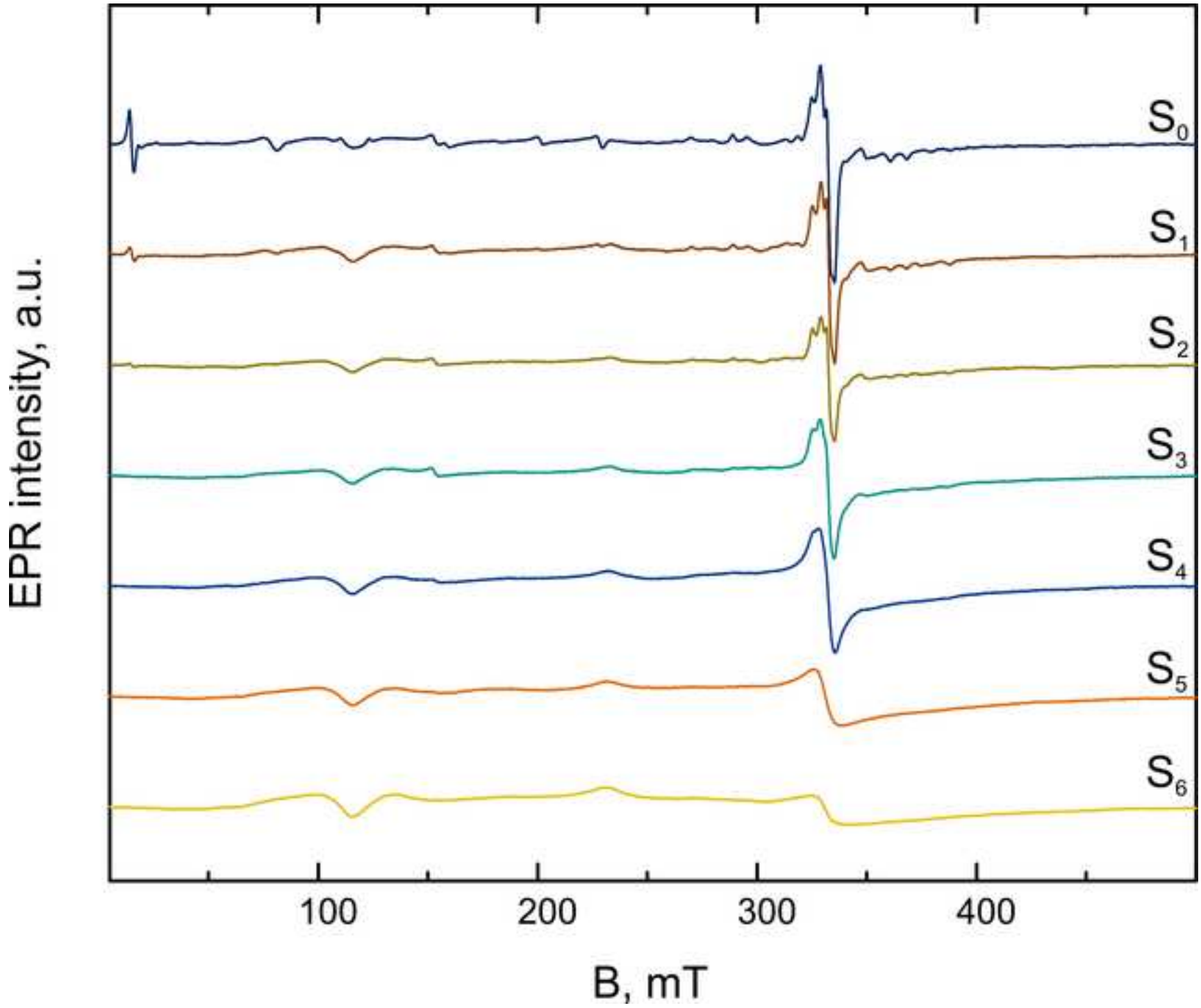

Figure 9

Click here to download high resolution image

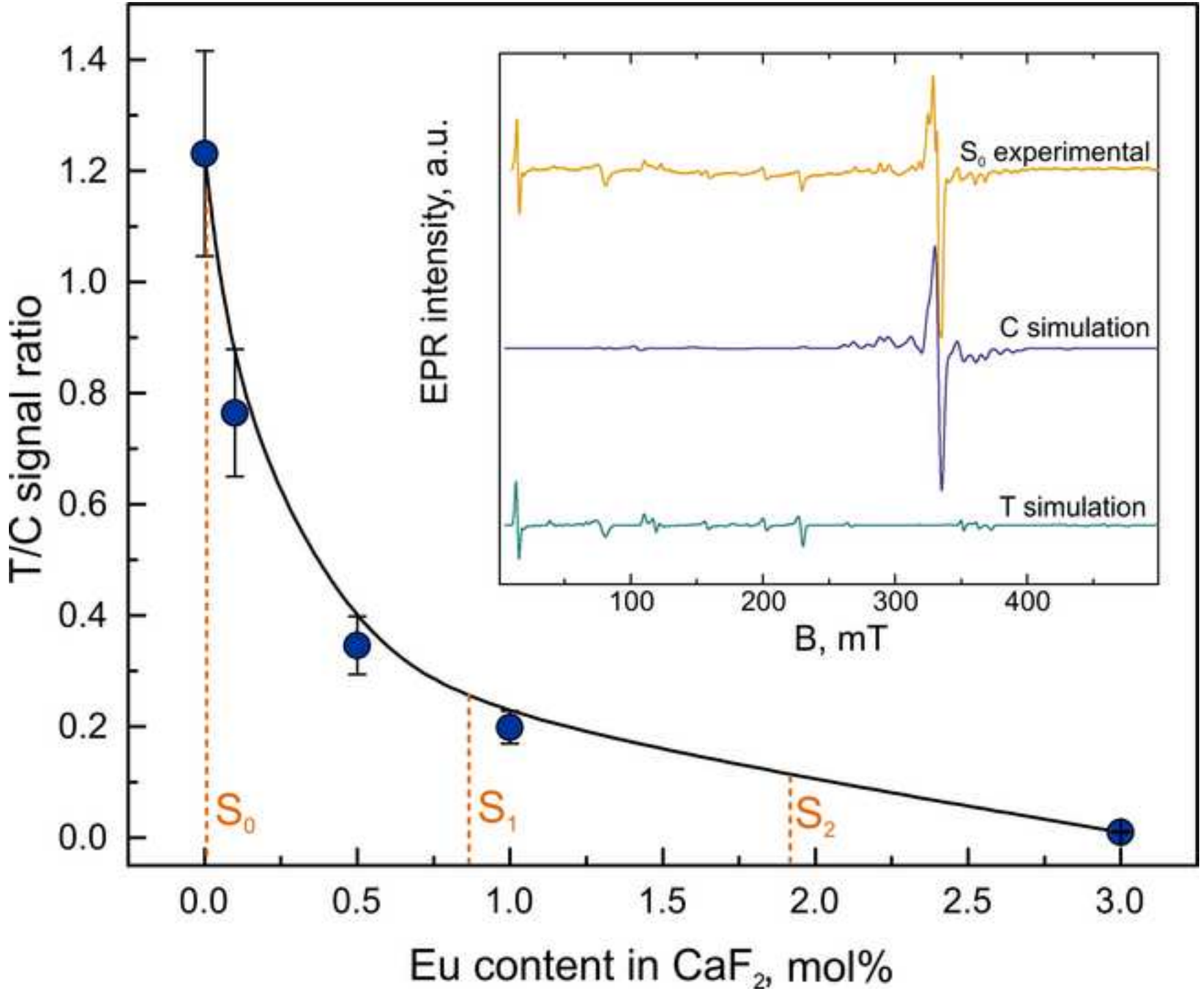

Figure 10

Click here to download high resolution image

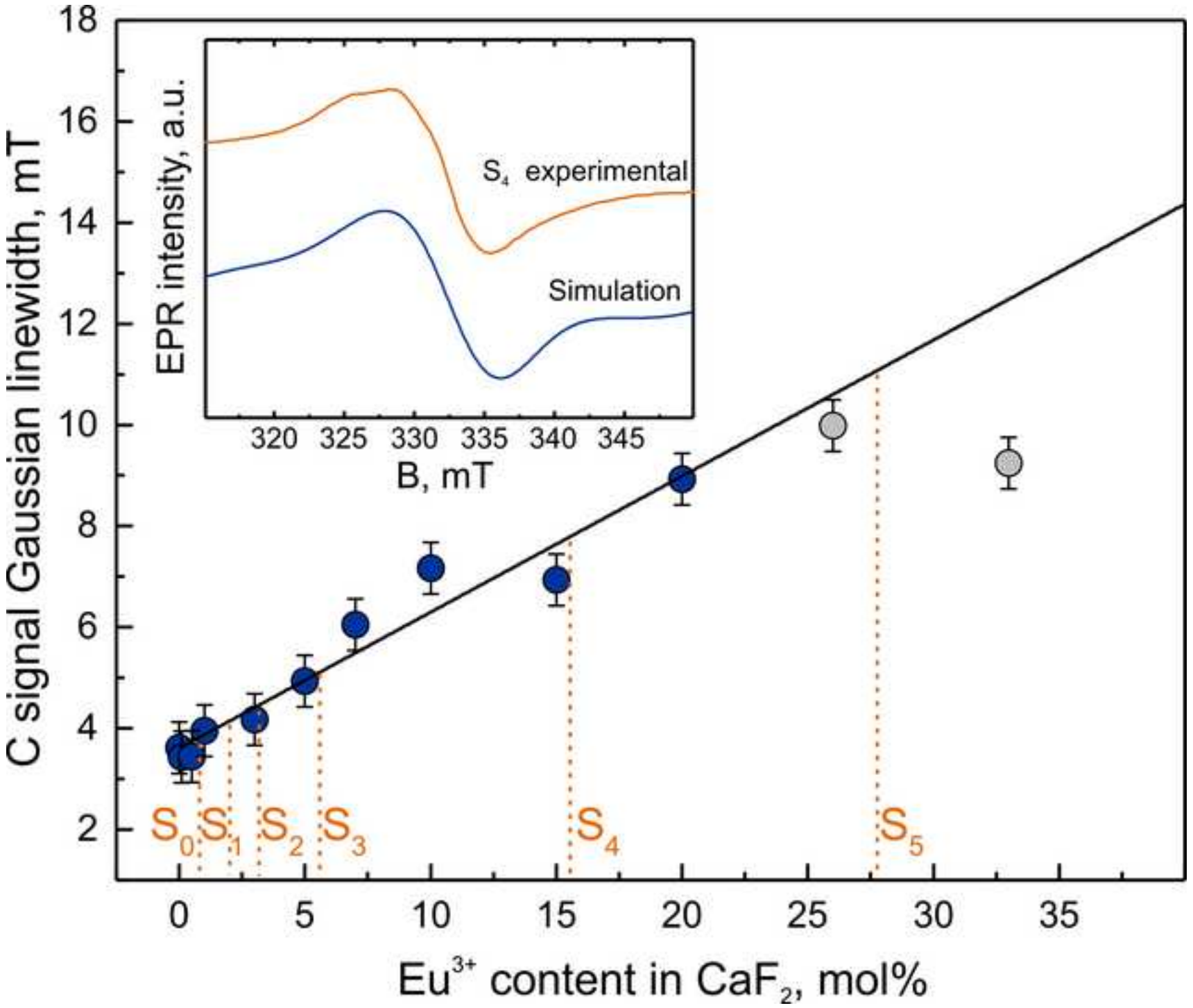

Figure R1 - for reviewers only, not to be included in final vers

Click here to download high resolution image

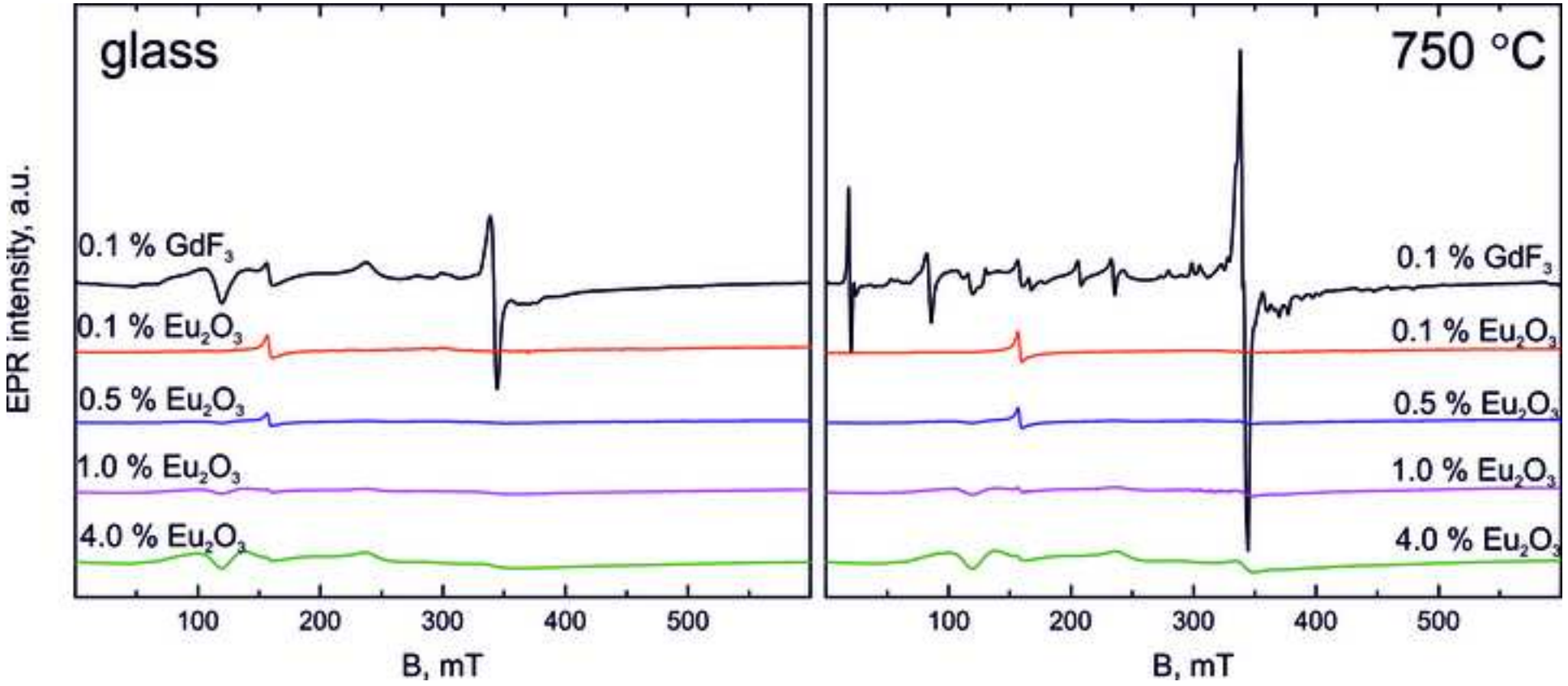

***Conflict of Interest form**

Conflict of Interest and Authorship Conformation Form

The following statements are valid:

- All authors have participated in (a) conception and design, or analysis and interpretation of the data; (b) drafting the article or revising it critically for important intellectual content; and (c) approval of the final version.

- This manuscript has not been submitted to, nor is under review at, another journal or other publishing venue.

- The authors have no affiliation with any organization with a direct or indirect financial interest in the subject matter discussed in the manuscript.

The corresponding author confirms on behalf of all authors that there have been no involvements that might raise the question of bias in the work reported or in the conclusions, implications, or opinions stated.

Andris Antuzevics

***Declaration of Interest Statement**

Declaration of interests

☒ The authors declare that they have no known competing financial interests or personal relationships that could have appeared to influence the work reported in this paper.

☐The authors declare the following financial interests/personal relationships which may be considered as potential competing interests: